THE EFFECT OF A MODERATOR SLAB ON A FAST NEUTRON BEAM

by

William Dale Leech

A Thesis Submitted to the
Graduate Faculty in Partial Fulfillment of
The Requirements for the Degree of
MASTER OF SCIENCE

Major Subject: Nuclear Engineering

Iowa State University
Ames, Iowa

1967

TABLE OF CONTENTS

		Page
I.	INTRODUCTION	1
II.	LIST OF SYMBOLS	5
III.	THEORETICAL DEVELOPMENT	7
IV.	EXPERIMENTAL ARRANGEMENT AND EQUIPMENT	17
	A. Neutron Generator	17
	B. T(D,n) Reaction	20
	C. Paraffin Slab	23
	D. Detector Foils	26
	E. Counting Technique	31
V.	RESULTS AND DISCUSSION	36
VI.	SUMMARY AND CONCLUSIONS	51
VII.	TOPICS FOR FURTHER STUDY	52
VIII.	LITERATURE CITED	54
IX.	ACKNOWLEDGMENTS	56

I. INTRODUCTION

In recent years the use of accelerator-type neutron sources has grown considerably. The accelerators offer a relatively inexpensive and easy method of producing neutron beams and pulses when compared to a reactor. The cost of an accelerator is far below that of a reactor, and the need for a sophisticated chopper is eliminated since pulsing can be performed electronically by deflecting the charged particles off the target.

With these accelerators it is possible to produce fast neutron beams or pulses. The commonly used D-D or D-T reactions give birth to high energy neutrons. Epithermal or thermal beams or pulses can also be produced by using the accelerator in conjunction with a moderating slab such as a paraffin slab.

Pulsed neutron studies have become a major subject of interest to nuclear engineers in the past few years. Pulsed neutron techniques have been used to make subcriticality measurements, thermal neutron diffusion parameter measurements, and investigations on many other important parameters.

Although it would be desirable to study the effect of a paraffin slab on a neutron pulse, which would allow the investigation of the time dependence of the outcoming spectrum, this work was confined to steady state measurements. Time

analysis equipment, which is highly expensive for analysis in the nanosecond range, was not available, and the inability of the neutron generator in its present form to yield very short pulses restricted these measurements to steady state condition.

This thesis contains the results of measurements of the epithermal neutron spectra that exit from a slab of paraffin when the slab is placed in front of a fast neutron source, such as the source produced at the target of a Texas Nuclear neutron generator.

Various methods are available for the measurement of neutron spectra. Some of these methods are time-of-flight measurements, activation analysis, proton recoil measurements using a Bennett spectrometer, semiconductor techniques, and threshold reactions. The choice of the method to be used depends upon the energy range to be investigated. Time-of-flight measurements (13) are generally used for spectrum measurements in the 0 to 100 eV range, but can be extended to higher energies with more sophisticated equipment. Semiconductor devices (7) and threshold reactions are generally used for spectrum measurements above 100 KeV. Proton-recoil measurements using a Bennett spectrometer are used for energies above 80 KeV (1). Activation analysis techniques are normally restricted to neutron energies below 1 KeV since difficulty is encountered in finding suitable materials with strong resonances above 1 KeV.

All the above mentioned techniques were considered in trying to determine which method should be used to measure the spectrum in question. Semiconductor and threshold reaction techniques were rejected because they cannot be used in the 1 to 500 eV region, which was the range of interest. Time-of-flight techniques could be extended to work up to 500 eV but there was not adequate space near the neutron generator to permit the long drift tube which is necessary for this method. Activation analysis seemed to be the only technique that would work under the desired conditions.

There are two different methods of obtaining spectrum measurements by activation analysis. They are the cadmium-ratio technique (12) and the sandwich foil technique (3). The former method is based on the assumption that the spectrum varies inversely with energy, i.e. it is proportional to 1/E. Since it was felt that this assumption was not warranted for the spectrum to be measured, the cadmium-ratio technique was abandoned in favor of the sandwich foil technique. There is no assumption placed on the shape of the spectrum in using the sandwich method.

The sandwich method involves foils of the same material, one placed on top of the other. The foil closest to the neutron source is black to neutrons at the resonance energy of the foil and therefore very few neutrons of this energy reach the second foil, while other neutrons are attenuated very

little in the first foil. The difference in activation of the two foils can then be used to determine the neutron flux at the resonance energy of the material. By using different materials with different resonance energies a spectrum measurement can be obtained.

II. LIST OF SYMBOLS

Symbol	Units	Meaning
A	neutrons/cm^2sec	Attenuation of neutrons in the foil
C_i	reactions/cm^2 sec	Reaction rate in the inner foil
C_o	reactions/cm^2sec	Reaction rate in the outer foil
E	eV	Energy of the exiting neutron
E_m	MeV	Maximum energy of the emitted β particle
E_{oi}	eV	Energy of the i-th resonance in the foil material
f_b		Back-scattering factor
f_s		Self-absorption factor for β particles
F_{ss}		Self-shielding coefficient
f_w		Absorption factor
f_τ		Dead time factor
G		Geometry factor
$I(M)$		Resonance activation function
K	neutrons/cm^2 sec	Neutron flux at a neutron velocity V and a neutron density ρ
M_C	gm/gm atomic wt	Atomic weight of carbon
M_H	gm/gm atomic wt	Atomic weight of hydrogen
M_i		Thickness of foil in mean free paths at the peak of the resonance
$\dot{m}$	cps, cpm	Measured count rate
N	atoms/cm^3	Number of atoms of foil material per unit volume

Symbol	Units	Meaning
P	reactions/cm^2 sec	Reaction rate of foil
P_{res}	reactions/cm^2 sec	Reaction rate due to resonance neutrons
s	cps, cpm	True count rate
t	cm, in.	Foil thickness
V	cm/sec	Neutron velocity
α		Mean probability for an isotropic flux that a neutron incident on the foil will be absorbed
Γ_i	eV	Total width of the i-th resonance in the foil
ε_β		Intrinsic detector efficiency for β particles
Θ	degrees	Angle between the perpendicular to the foil and the direction of incidence of the neutron on the foil
μ_m	cm^2/gm	Mass absorption coefficient
ρ	neutrons/cm^3	Neutron density
Σ_a	cm^{-1}	Macroscopic absorption cross section
Σ_t	cm^{-1}	Total macroscopic cross section
σ_a	barns	Microscopic absorption cross section
τ		Thickness of foil in mean free paths
ϕ	neutrons/cm^2 sec eV	Neutron flux
Ω	steradians	Solid angle

III. THEORETICAL DEVELOPMENT

One of the earliest theoretical treatments of neutron absorption in a thin foil was done by Bothe (2). In this treatment he obtained the activity which is produced when a foil is placed in a neutron flux. The following treatment follows the same line of reasoning as that used by Bothe.

If a foil is placed in a neutron flux the neutron density is given by

$$\rho = \frac{1}{V} \int K d\Omega \qquad (1)$$

The absorption per unit solid angle is then

$$dA = K \mid \cos \Theta \mid (1 - e^{-\frac{\sigma_a t}{\cos \Theta}}) d\Omega \, . \qquad (2)$$

At this point it is necessary to make some assumption as to the spatial distribution of the flux. It was assumed that the flux is isotropic on the side of the foil facing the neutron source and no neutrons impinge on the other side of the foil (see Figure 1). The flux can then be written as

$$K = K_o \qquad 0 \leq \Omega \leq 2\pi$$

$$K = 0 \qquad 2\pi \leq \Omega \leq 4\pi \, .$$

The total neutron density can then be written from Equation 1.

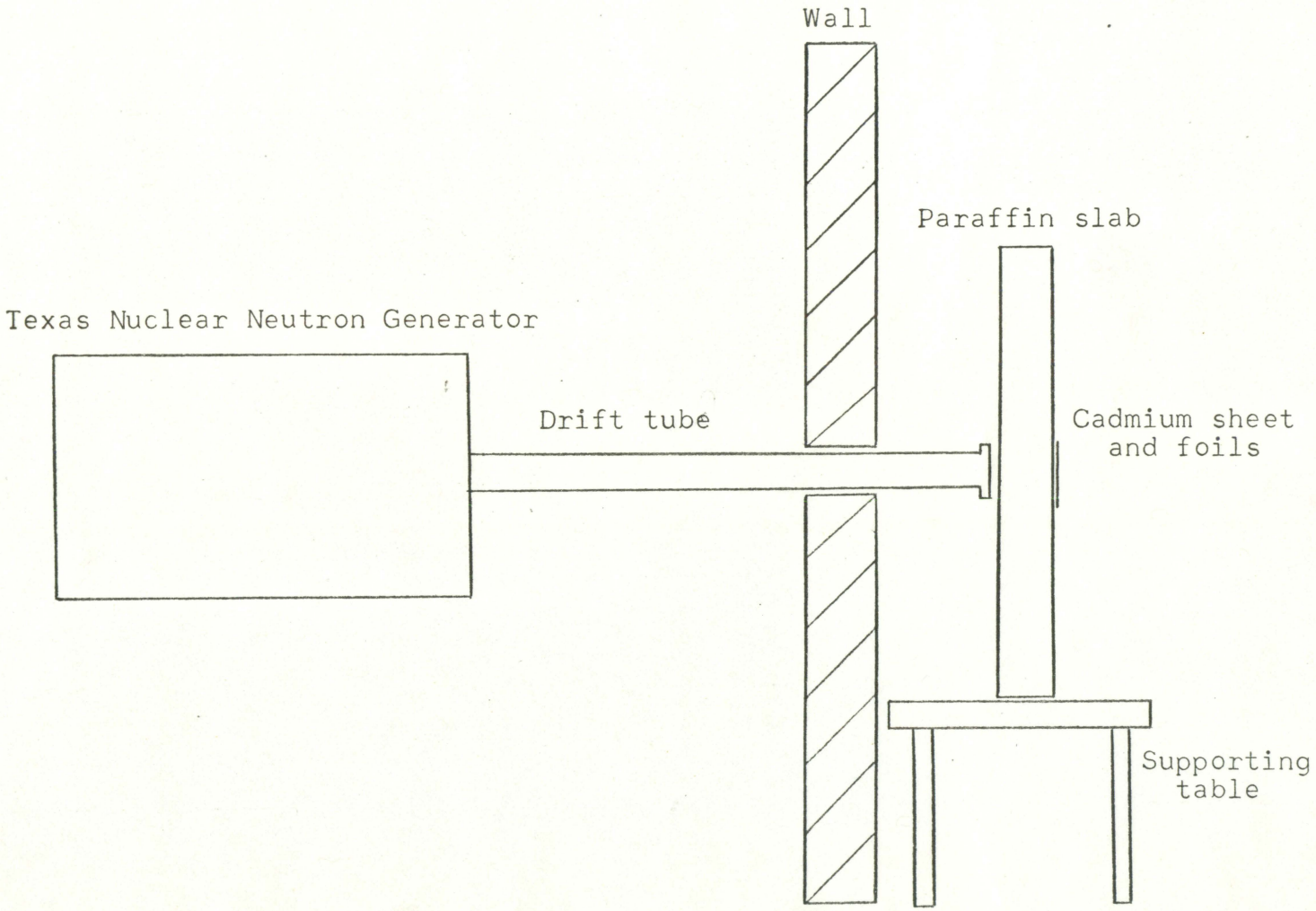

Figure 1. Experimental arrangement

$$\rho = \frac{1}{V} \int_0^{2\pi} K_o d\Omega \ . \tag{3}$$

$$\rho = 2\pi \frac{K_o}{V} \ . \tag{4}$$

The total absorption becomes

$$A = 2\pi K_o \int_0^1 \cos\theta \left[1 - e^{-\frac{\Sigma_a t}{\cos\theta}}\right] d(\cos\theta) \ . \tag{5}$$

Substituting for K_o from Equation 4

$$A = \frac{1}{2} V\rho \left[1 - e^{-\Sigma_a t}(1 - \Sigma_a t) + \Sigma_a^2 t^2 E_i(-\Sigma_a t)\right] , \tag{6}$$

where E_i is a function tabulated in (8). The following variable was defined:

$$\alpha = \frac{2A}{V\rho} = 1 - e^{-\Sigma_a t}[1 - \Sigma_a t] + \Sigma_a^2 E_i(-\Sigma_a t) \ . \tag{7}$$

Recalling that $\tau = \Sigma_a t$ for a pure absorbing material α may be expressed as

$$\alpha = 1 - 2\, E_3(\tau) \ , \tag{8}$$

where

$$E_3(\tau) = \frac{1}{2}\left[(1 - \tau)e^{-\tau} + \tau^2 E_1(\tau)\right] \ . \tag{9}$$

With the use of Equation 8 it is now possible to obtain

a relation which yields the reaction rate in a foil exposed to the assumed neutron flux. The following treatment was developed by Judd (8). It should be noted that the expression obtained for α in this case is the same as in the case of isotropic flux.

The reaction rate in a small foil placed in a neutron flux is given by

$$P = \int_E F_{ss}\tau(E)\phi(E)dE \ . \qquad (10)$$

F_{ss} is called the self-shielding coefficient. This coefficient takes into account the fact that the flux is lower in the center of the foil than near the surface due to the absorption of neutrons in the outer layers. F_{ss} can be expressed as

$$F_{ss} = \frac{\alpha}{2\tau} \ . \qquad (11)$$

It should be noted that in Equation 10 there is usually an additional term that accounts for the lowering of the flux due to the introduction of a neutron sink into the medium. This term is not present in this development since the foil is not in the medium and therefore does not perturb the flux at all.

The reaction rate in a foil which has a single absorption resonance and a zero cross section at all other energies

except the resonance energy is given by

$$P_{res} = \int_0^\infty F_{ss}\tau\phi dE \ . \tag{12}$$

Substituting from Equation 10 and assuming that the flux is constant across the resonance gives

$$P_{res} = \tfrac{1}{2}\phi \int_0^\infty \alpha dE \ . \tag{13}$$

The resonance absorption cross section is given by the Breit-Wigner formula

$$\sigma_a(E) = \pi\lambda_o^2 g\left(\frac{E_o}{E}\right)^{\frac{1}{2}} \frac{\Gamma_n\Gamma_\gamma}{(E - E_o)^2 + (\frac{1}{2}\Gamma)^2} \ . \tag{14}$$

Substituting of $\sigma_a(E)$ from Equation 14 into Equation 12 and assuming that $\Gamma << E_o$ (which implies $\frac{E_o}{E} = 1$) one obtains

$$P_{res} = \tfrac{1}{4}\phi\Gamma \int_{-\infty}^{\infty} [1 - \frac{2E_3(M)}{1 + \eta^2}]d\eta \ , \tag{15}$$

where

$$\eta = \frac{2}{\Gamma}[E - E_o]$$

$$M = t\Sigma_{a\ max} = tN \cdot 4\pi\lambda_o^2 g \frac{\Gamma_n\Gamma_\gamma}{\Gamma^2} \ .$$

The lower limit on the integral should be $\frac{-2E_o}{\Gamma}$ but the error in replacing this by $-\infty$ is small because the integrand is negligible for large $|\eta|$. Equation 15 can be written in a different form by making the following substitution:

$$I(x) = \int_{-\infty}^{\infty} 1 - 2E_3 \frac{x}{1 + y^2}\, dy \ . \qquad (16)$$

I(x) has been evaluated numerically and is shown in (8). Equation 15 then becomes

$$P_{res} = \tfrac{1}{4}\phi\Gamma I(M) \qquad (17)$$

To this point the resonance was considered to be pure absorption. Equation 17 must be modified to account for scattering resonances that sometimes accompany the absorption resonance. When this is done, Equation 17 becomes

$$P_{res} = \tfrac{1}{4}\phi\Gamma_\gamma I(M) \qquad (18)$$

where

$$M = t\Sigma_{t\ max} = N \cdot 4\pi\lambda\!\!\!^{-2}_{o} g \frac{\Gamma_n}{\Gamma} \ .$$

Equation 18 gives the reaction rate of a foil which has one resonance of width Γ_γ. The total macroscopic cross section is $\Sigma_{t\ max}$ and the thickness of the foil is t. ϕ is the flux at the resonance energy.

Materials with a cross section as assumed above do not

exist in nature. The fact that the cross section is not zero at energies other than the resonance energy must be taken into account in the choice of detector materials. The choice must also be made taking into account that one should be able to obtain thin foils of about five thousandths of an inch thick. In general the density of these materials is approximately ten and their atomic weight 100. This makes $\Sigma_t t \sim 0.001\sigma$, where σ is in barns. By choosing materials which have a cross section of less than 100 barns except at the resonance, $\Sigma_t t \sim 0.1$ and the foils can be considered thin except at the resonance. If this is the case Equation 10 can be written in the following form:

$$P = \int_{\text{non-resonance}} \tau \phi dE + \sum_i P_{\text{res } i} \qquad (19)$$

In this equation the first term on the right applies at all energies except at the resonances. The self-absorption term is omitted because the foils are considered thin and this term would be almost equal to one. The second term is the reaction rate due to the resonances. The summation is used if there is more than one dominant resonance.

The discussion up to this point has been on resonance detectors in general. No requirements or restrictions on how the foil is to be used have been made. The results to this point, expressed by Equations 18 and 19, yield what the

reaction rate of a foil would be when subjected to a neutron flux. To obtain a spectrum measurement some means must be devised to separate the measured reaction rate into the two terms on the right side of Equation 19.

Sandwiching of the foils is done to separate the non-resonance activation from the activation caused by absorption at the resonances. Two foils of the same size, thickness, and material are used to separate the two terms in Equation 19. The foils are placed against the moderating slab so that one foil is directly on top of the other. The foil closest to the slab is black to the resonances neutrons so that very few are able to travel through the first foil into the second. The first foil is also thin enough so that there is little attenuation of all other neutrons as they travel through it, and therefore the reaction rate from these non-resonance neutrons should be nearly the same in both foils. Thus the difference in reaction rate between the inner foil, closest to the slab, and the outer foil is due to the absorption of almost all resonance neutrons by the inner foil. Ehret (3) shows that 95 to 100% of the difference between the two reaction rates is due to resonance absorption in the inner foil. This difference in reaction rate can be used to obtain the neutron flux at the resonance energy.

Several different materials were used with their resonances at different energies and thus a spectrum was obtained

from the measured fluxes at these different resonances.

The two foils having the same shape and thickness were sandwiched together and placed against the paraffin slab. The reaction rate per unit area in the foil closest to the slab was, according to Equation 19

$$C_{inner}(t) = P(t) = \int_{non\text{-}res} \Sigma_a t \phi dE + \sum_i P_i(t) \ . \qquad (20)$$

The reaction rate in the outer foil was

$$C_{outer}(t) = P(2t) - P(t) = \int_{non\text{-}res} \Sigma_a 2t \phi dE + \sum_i P(2t)$$

$$- \int_{non\text{-}res} \Sigma_a t \phi dE - \sum_i P_i(t) \ . \qquad (21)$$

When Equation 21 is subtracted from Equation 20 the integral terms cancel each other and after substituting for P_{res} from Equation 17 the result becomes

$$C_i - C_o = \frac{1}{4} \sum_i \phi_i \Gamma_{\gamma i} [2I(M) - I(2M)] \ . \qquad (22)$$

This is the expression which was used to analyze the experimental data. The activities of the outer and inner foils were measured and then corrected to saturation activities. The saturated activities were equal to the reaction rates of the foils. The difference between the saturated

activities was used in Equation 22. When there is only one major resonance in the cross section of the detector material the summation may be dropped. Γ_γ was obtained from BNL-325 (4, 5, 6) and I(M) and I(2M) were obtained from Judd (8). Thus it was possible to solve for the flux at the resonance energy. The experiment was carried out with several materials with different resonance energies. The flux was then obtained at these energies and a spectrum for the neutrons coming out of the slab was plotted.

IV. EXPERIMENTAL ARRANGEMENT AND EQUIPMENT

The analysis presented in Chapter III enables one to determine the neutron spectrum in the energy region 1 to 350 eV. In this Chapter the experimental arrangement and equipment which was used is discussed. The experimental arrangement is shown in Figure 1.

A Texas Nuclear Neutron Generator was used to produce fast neutrons. Those neutrons that exited from the target in a forward direction passed through the paraffin slab. Three different slabs of thickness 1.25 in., 1.875 in., and 2.50 in. were used. On the back of the slab was mounted a 0.020 in. sheet of cadmium to which four foil sandwiches were attached. The foil materials were, in the order of their dominant resonance energy, In, Au, W, Mn. After the irradiation was completed the foils were removed and their activity counted in a 2π gas flow detector.

The various components of the experiment will now be discussed in detail.

A. Neutron Generator

A model 9500 neutron generator produced by Texas Nuclear Corporation was used (11). The basic components of the generator are shown in Figure 2.

The ion source section is responsible for the production, extraction, and focusing of deuterium ions. The ion source

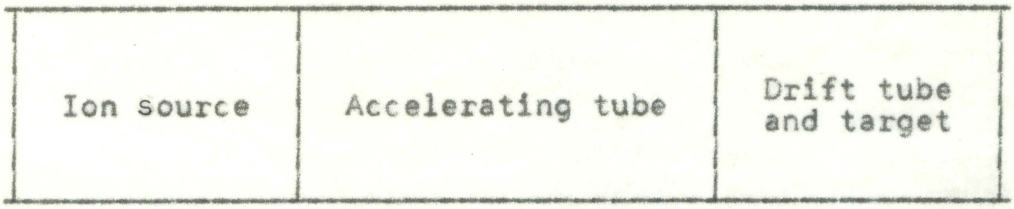

Figure 2. Block diagram of the neutron generator

is an improved radio frequency source developed at Oak Ridge National Laboratory. A radio frequency field causes intense ionization of the deuterium gas. With this type of equipment 90% of the ions produced are singly ionized atomic ions. The ion source consumes approximately 20 cc of gas per hour. The positive ions are forced out of the ionizing region by a positive potential, and after being focused, enter the accelerating tube.

The accelerating tube accelerates the ions to 150 KV. This acceleration is accomplished by ten acceleration steps of 15 KV each.

The high velocity ions leaving the acceleration section travel down a drift tube and strike the target. The entire system is held at a pressure of 2×10^{-5} mm of Hg to decrease the collisions of the ions with gas in the drift tube. The target assembly is water cooled and consists of tritium or deuterium gas occluded in a thin layer of titanium. An electron suppressor is also present near the target. This

device causes electrons that are produced during the bombardment of the target to return to the target. If this suppressor were not present erroneous readings of the beam current would result.

Neutrons are produced by one of two different reactions. These reactions are

$$ {}_1H^2 + {}_1H^3 \rightarrow {}_2He^5 \rightarrow {}_0n^1 + {}_2He^4 + 17.6 \text{ MeV} \qquad (23) $$

$$ {}_1H^2 + {}_1H^2 \rightarrow {}_2He^4 \rightarrow {}_0n^1 + {}_2He^3 + 3.25 \text{ MeV} . \qquad (24) $$

The neutron yield from the D-T reaction, Equation 23, is about 100 times greater than the D-D reaction yield. The tritium reaction was used in the experiments because neutron fluxes as high as possible were desired.

The target has what is known as a half-life. This is the operating time it takes for the neutron yield to drop to one-half its original value. This drop in yield is caused by the consumption of the tritium in the target. This half-life is a function of the ion current. For a steady state operating condition of 1000 microamps ion current the half-life of the target is two hours. For an ion current of 500 microamps the half-life is four hours.

B. T(D,n) Reaction

The Q value of the tritium reaction is 17.6 MeV. This energy plus the initial kinetic energy of the deuteron is shared by the neutron and the α particle that are formed. A neutron emitted in the same direction as the direction of travel of the incident deuteron has an energy of 14.7 MeV. The remaining 3.05 MeV goes as kinetic energy to the α particle and is dissipated as heat when the α particle is stopped in the target.

The number and energy of the out going neutrons depends on the angle at which the neutron leaves with respect to the initial direction of the deuteron. The departure from isotropic distribution is not large. Table 1 shows the relative neutron yield as a function of Θ which is defined as the angle between the exit direction of the neutron and the direction of the incident deuteron. Table 2 shows the energy of the neutron as a function of Θ. Tables 1 and 2 are combined in Figure 3 to give a plot of number of neutrons versus energy of neutrons. If it is assumed that only those neutrons that leave the target at an angle of $\pm 30^{\circ}$ or less reach the foils, the energy spread of the initial spectrum, from Table 2, is 14.65 MeV to 14.74 MeV. The spread in the relative yield is shown on Figure 3.

During the experiment the neutron generator was operated at a steady ion current of 500 microamps. This is fifty per-

Table 1. Neutron yield versus angle

θ (degrees)	Neutron yield (relative to 0°)
0	1.00
60	0.97
90	0.94
120	0.91
150	0.88
180	0.87

Table 2. Neutron energy versus angle

θ (degrees)	Neutron energy (MeV)
0	14.74
15	14.72
30	14.65
45	14.54
60	14.40
75	14.23
90	14.06
105	13.89
120	13.74
135	13.61
150	13.51
165	13.44
180	13.42

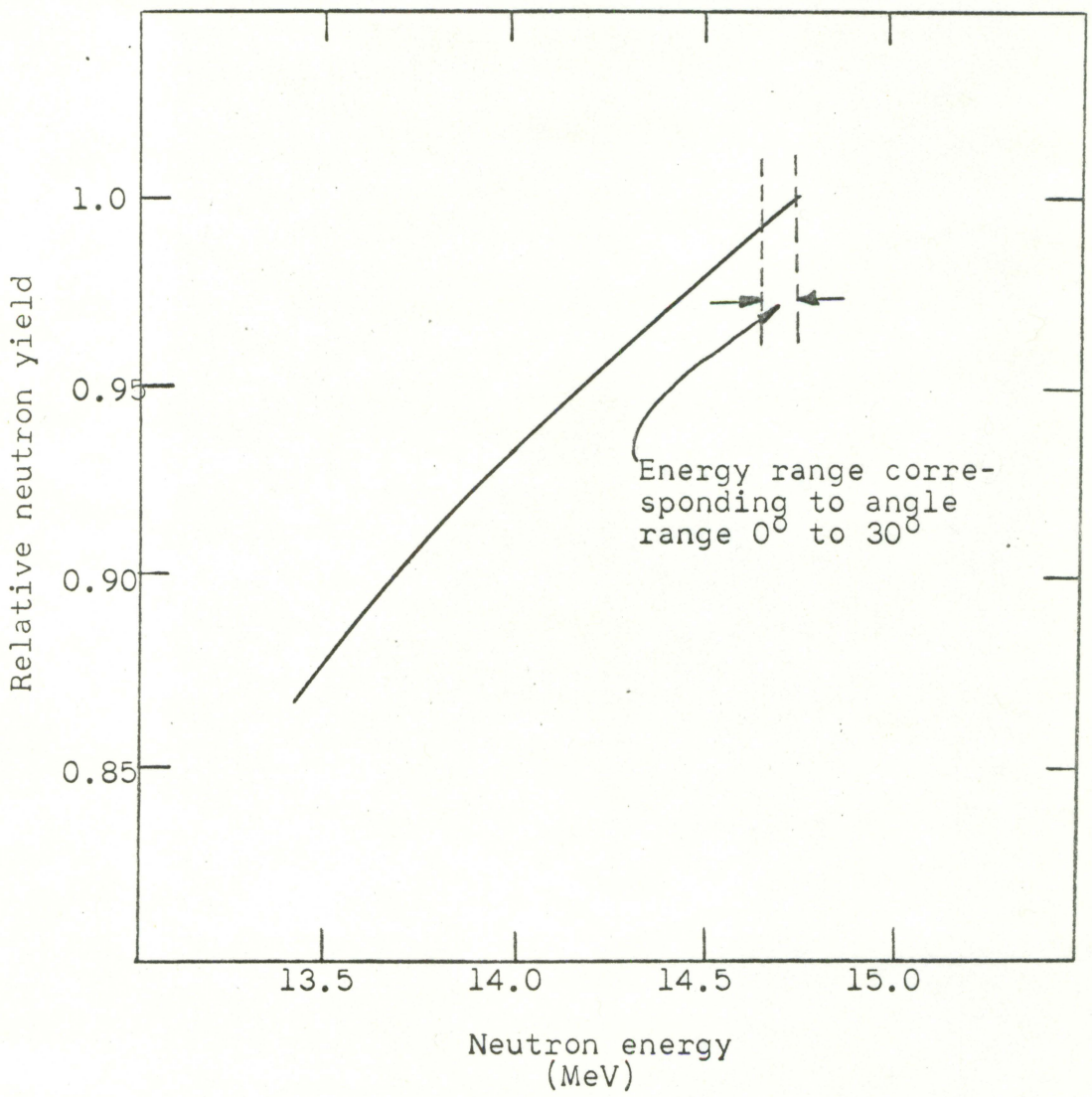

Figure 3. The dependence of neutron yield on neutron energy

cent of the rated capacity of the generator. The irradiation time was thirty minutes.

C. Paraffin Slab

Paraffin was chosen as a moderating material to slow down the neutrons because of its high hydrogen content, availability, and ease of fabrication. Water was also considered as a possible moderating material but was rejected because of the necessity of a tank to contain it. It was felt that the tank would interfere with the measurements. Also, measurements were to be carried out at several slab thicknesses which would have required several tanks.

The paraffin slab was constructed by melting paraffin into a mold. This allowed the slab to be free of voids and uniform in consistency. Building the slab by assembling smaller blocks was rejected because of the voids and gaps that would have been present with this method of construction. The original slab was 22 in. square by 2.5 in. thick. Measurements were carried out at this thickness and then the slab was thinned to 1.875 in. and finally to 1.25 in. Spectrum measurements were carried out at these new thicknesses to determine the effect of varying slab thickness on the outcoming spectrum.

The width and height of 22 in. was chosen because it was felt that this dimension was sufficient to approximate an

infinite slab. The height of 22 in. also allowed the slab to be placed on a small table in such a manner that the center of the slab was located directly in front of the target of the neutron generator. It was felt that this geometrical configuration was necessary due to the manner in which the foils were attached. The attachment of the foils is discussed in the following section.

It was desirable to know the dimensions of the slab in terms of the scattering mean free path. To determine this it was necessary to know the atomic densities of the hydrogen and carbon in the paraffin. The atomic densities could have been determined if the density and the molecular weight of the paraffin had been known. The density was measured with no difficulty, but the molecular weight presented a problem.

The word paraffin refers to any saturated aliphatic hydrocarbon with the general formula C_NH_{2N+2}. In commercial paraffin the value of N in the general formula is not a constant. In a given piece of paraffin the value of N may vary greatly. It is therefore very difficult to determine a molecular weight of a commercial sample of paraffin.

In order to determine the atomic densities it was assumed that the paraffin had a formula of C_NH_{2N}. Ignoring the two hydrogen atoms should introduce an error of not more than 2% since the value of N was around fifty. With this assumption the atomic densities were calculated without

knowing the value of N.

The density of the paraffin was measured and found to be 0.9225 g/cm^3. The weight of hydrogen per cc was then obtained.

$$0.9225\left[\frac{2M_H}{2M_H + M_C}\right] = 0.9225\left(\frac{2.016}{14.02}\right) = 0.1328 \text{ g/cm}^3 .$$

The number of hydrogen atoms per cm^3 was then found by dividing the weight of the hydrogen per cm^3 by the weight of a hydrogen atom.

$$\text{Hydrogen atoms/cm}^3 = \frac{(0.1328)(6.02 \times 10^{23})}{(1.008)} = 7.92 \times 10^{22} .$$

In the same manner the carbon atomic density was found to be 3.98×10^{22} atoms per cm^3.

The scattering cross sections of hydrogen and carbon at the energy of the incoming neutrons, i.e. 14.7 MeV, are 0.69b and 1.35b respectively. From the atomic densities and the cross sections the scattering mean free path can be calculated.

$$\lambda_s = \frac{1}{N_H \sigma_{sH} + N_C \sigma_{sC}}$$

$$= \frac{1}{0.69 \times 10^{-24}\text{cm}^2 \times 7.92 \times 10^{22} \frac{\text{atoms}}{\text{cm}^3} + 1.35 \times 10^{-24}\text{cm}^2 \times 3.98 \times 10^{22} \frac{\text{atoms}}{\text{cm}^3}}$$

$$= 9.2 \text{ cm} .$$

With this value for λ_s the thickness of the three slabs in

scattering mean free paths were 0.69, 0.518, and 0.345.

The paraffin slab was placed on a small table directly in front of the target. Care was taken so that the center of the slab face was directly in front of the target center. A gap of approximately 0.25 in. was left between the target assembly and the slab.

D. Detector Foils

The face of the paraffin slab facing the target where the fast neutrons originate will be referred to as the front face while the opposite face from which the moderated neutron beam exits will be referred to as the back face. A 5 in. by 5 in. sheet of cadmium 0.020 in. in thickness was placed on the back face centered on the axis of the accelerator beam. The cadmium sheet and the attached foils are shown in Figure 4. The cadmium sheet was used to eliminate thermal neutrons coming out from the slab which would have otherwise struck the foils. The cadmium sheet has little effect on the epithermal neutrons while it absorbs almost all thermal neutrons which would induce additional activity in the indium foil because of the latter's high thermal cross section.

Four materials were used in a sandwich form: In, Au, W, and Mn. The sandwiches were made by placing two foils of the same material on top of a small piece of aluminum

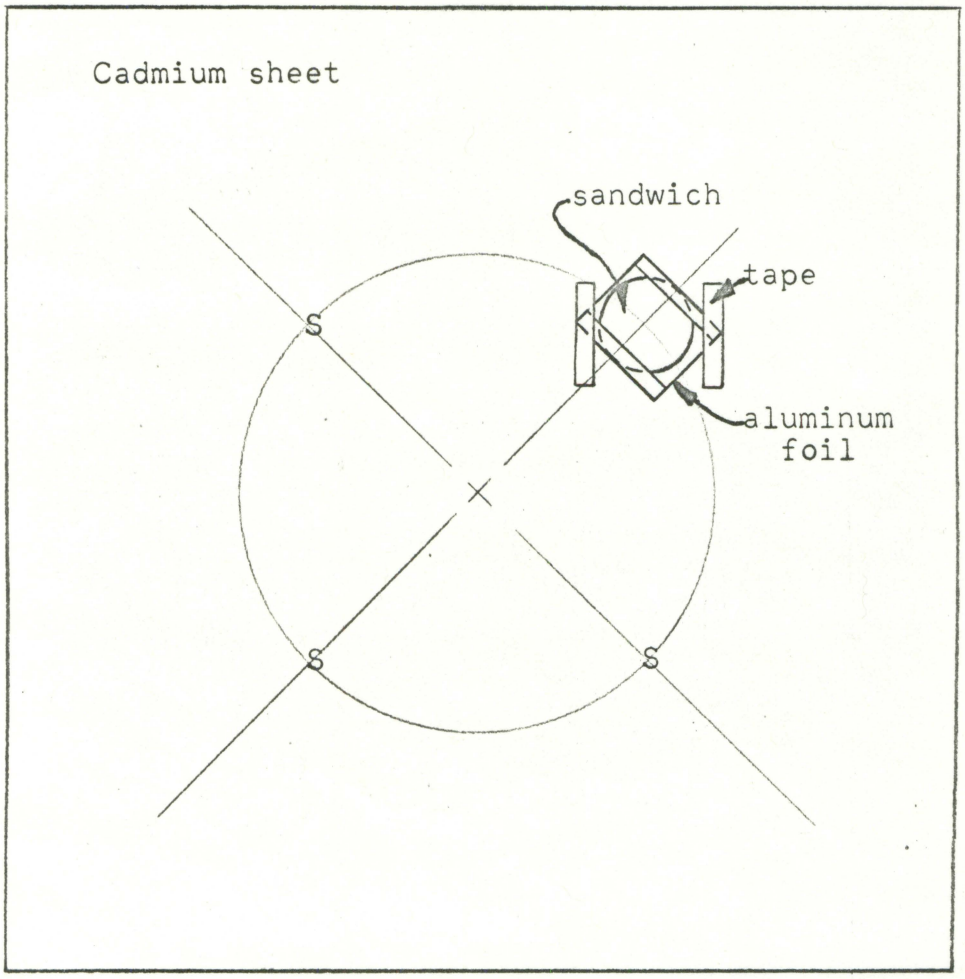

Note: S denotes other three sandwich locations

Figure 4. View of the resonance foils and cadmium sheet as attached on the paraffin slab

foil. The aluminum foil was then folded over the corners of the sandwich material. Care was taken so that the two identically shaped foils remained exactly on top of each other. The four sandwiches were fastened to the cadmium sheet with tape as shown in Figure 4. The foils were attached to the cadmium on the periphery of a circle of 1.25 in. radius centered on the axis of the beam. In this manner the distance from each sandwich to the target was the same.

The choice of foil material was made on the basis of many parameters. The material should have a dominant resonance and a low cross section (less than 100b) at all energies except at the resonance energy. The material should also be obtainable in the form of thin foils. The product nuclide after neutron absorption must be radioactive, i.e. the material should activate. This product nuclide should have a short enough half-life to enable sufficient count rates to be obtained. The radioactivity produced should be of a type that can be measured with a fair degree of ease.

When all of these criteria are taken into account the number of materials suitable for this kind of work is very small. Lanthanum and cobalt are about the only other suitable materials that could be used besides the ones already mentioned. Lanthanum has the undesirable property of oxidizing rapidly in air and therefore it must be handled under inert atmosphere. For this reason lanthanum was not used

in the experiments. Cobalt has the disadvantage of having a half-life too long to allow appreciable count rates to develop under the conditions of the experiment and therefore was also eliminated. Table 3 gives the basic parameters of the foils that were used.

As can be seen from Table 3 the manganese was much thicker and had a different shape than the other foils. The first three foils were punched from thin sheets of their respective materials, but the two manganese foils were made by grinding down by hand two small pieces of this material. Due to the extreme brittleness of manganese it was impossible to obtain thinner foils by this technique. It should be noted that even though the manganese foils were much thicker than the other foils, the manganese was still thin (as defined in Chapter III) at energies other than its resonance. This was due to the cross section of manganese being less than twenty barns at almost all energies other than its resonance energies. The dimensions of the manganese foils are shown in Figure 5.

All four materials used produce β-emitters by neutron activation. After the irradiation by the neutron generator the foils were removed from their aluminum jackets and the beta activity was counted.

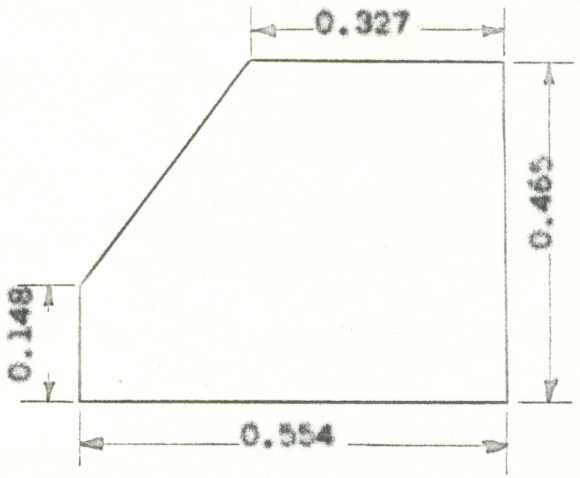

Note: All dimensions in inches

Figure 5. Manganese foils

Table 3. Foil material parameters

Material	Thickness (in.)	Size (in.)	Resonance energy (eV)	Height of resonance (b)	Half life
In	0.002	0.5 dia.	1.456	30,000	55 min
Au	0.001	0.5 dia.	4.906	30,000	2.7 d
W	0.001	0.5 dia.	18.8	14,000	24 h
Mn	0.024	irregular	337	3,400	2.55 h

E. Counting Technique

The activity of the foils was counted using a Model D-47 Gas Flow Detector. The detector was used as a 2π proportional counter. A mixture of 10 percent methane and 90 percent argon was used for gas in the detector. The operating voltage for the detector was 2050 volts.

The output signal from the detector was fed to a Model D-47P Preamplifier and then to a Model 186 Decade Scaler. The gain on the preamplifier was 5.0. The detector, preamplifier, and scaler were all manufactured by Nuclear Chicago Corporation.

It is necessary to take absolute count rate measurements of the radioactive foils if an absolute spectrum is to be determined by the sandwich foil technique. When absolute count rates are obtained for the foils the spectrum that is determined is correct in amplitude as well as in shape.

If the absolute magnitude of the flux is not of concern and all that is desired is the shape of the flux distribution, absolute counting is not necessary. The shape of the spectrum can be determined if the various foils are measured in such a way that their relative activities are determined correctly. For example, if absolute activities are to be measured, it is necessary to determine a geometry factor for the counting equipment used and correct the measured activity by

this factor. If measurement of relative activities is adequate, it is only necessary to keep the geometry constant in all foil activity measurements. By doing this the geometrical correction factor is the same for all the foils. The objective of this thesis was to determine the shape of the spectrum exiting from the paraffin slab. The absolute height or magnitude of the flux was not of interest. Therefore, it was not necessary to determine absolute count rates for the radioactive foils. Relative counts were taken instead and various corrections were made to insure that the count rates from the different foil materials were correct relative to each other. The corrections are shown in Equation 25 (10).

$$s = \dot{m}/G\varepsilon_{\beta}f_{\tau}f_{w}f_{b}f_{s} \cdot \qquad (25)$$

Since relative count rates are of interest the factors which were the same for all the foils were not taken into account. The geometry factor was made the same for all the foils. This was done by placing the foils in the same location each time a count was made. The distance from the top surface of the foil was held constant for all the foils. The shape of the foils was identical except in the case of the manganese and even in this case the deviation from the shape of the others was small.

The intrinsic efficiency of the detector for β particles

was assumed to be a constant.

The resolving time of the gas flow counter was 6 μsec. This was the maximum resolving time in the equipment. The correction for dead time was less than one percent for the maximum count rate observed and therefore this factor was ignored.

The factor f_w was the correction factor due to absorption between the foil and the sensitive volume of the counter. This absorption included absorption in the air gap between the foil and the sensitive volume and the Mylar window which separates the two. The air gap was approximately 1/32 in. and the thickness of the Mylar window was 0.150 mg/cm^2. Under these conditions this factor was constant for the various foils.

The source mount backscattering factor, f_b, accounted for those β particles which were scattered from the backing on which the foil was placed into the sensitive volume of the detector. This term was a function of the energy of the β particles, the thickness of the material used for the backing, and the atomic number of the backing material. Aluminum was used for backing during the counting of the foils. Taking this into account and the energies of the various β particles, this term was assumed nearly constant for the various foils. This assumption was very close to reality and facilitated the analysis of the data since it was difficult to measure this factor

experimentally for each foil.

The factor f_s was used to correct for the absorption of β particles by the foil itself. An attempt was made to measure this term experimentally by placing foil material on top of a radioactive foil and measuring the decrease in observed counting rate. A straight line should appear on semilog paper when the measured activity is plotted versus total thickness of foil material (10). From the slope of this line f_s can be determined. This experiment failed due to the excessive thickness of the foils. Thinner foils, which were not available, were necessary to determine f_s experimentally.

A theoretical expression for f_s was then used from Price (10).

$$f_s = \frac{1}{\mu_m t}[1 - e^{-\mu_m t}] . \qquad (26)$$

The factor μ_m has been found to follow the following emperical relationship:

$$\mu_m = \frac{17}{E_m^{1.14}} . \qquad (27)$$

Equations 26 and 27 were used in conjunction with the decay schemes of the various foil materials and the values of f_s were calculated. These values are shown in Table 4.

Of all the factors in Equation 25, f_s was the only one that could not be made equal for all the foil materials by

Table 4. Self absorption factor for β particles

Material	f_s
In	0.698
Au	0.670
W	0.562
Mn	0.254

appropriate choice of distance, backing material, and detector type. The measured foil activities had to be divided by the appropriate f_s to yield correct relative counts. When this was done the exiting spectrum shape was obtained from the data points corresponding to the various foils.

V. RESULTS AND DISCUSSION

In this Chapter the experimental data will be presented; the processing of the data will be explained and the neutron spectra exiting from the paraffin slab will be shown. In the final portion of this Chapter the results will be discussed and compared to results obtained by others.

After the irradiation the foils were removed from the cadmium sheet and counted in the gas flow detector. Both foils in each sandwich were counted separately. Sample data are shown in Table 5.

It was desired to obtain count rates for the foils at a zero sensitivity setting on the scalar discriminator. This was necessary because the relative count rates for the different foils would not be correct at discriminator settings other than zero due to the differences in the β particle energies of the different activated foil materials. Since it was impossible to get accurate counting rates below a discriminator setting of about 2.5 mV due to amplifier noise, data were taken at various non-zero discriminator settings and the straight line that fitted them best was then extrapolated back to zero discriminator setting.

The processing of the data for one foil is shown in Table 6. These data are those for indium taken from Table 5. The observed counting rates were corrected for background. The

Table 5. Sample data

Time of start of irradiation	-	9:05 AM
Time of end of irradiation	-	9:35 AM
Paraffin slab thickness	-	0.345 λ_s
Background counts for 20 minutes	-	308

Outer foil			Inner foil	
		Indium		
Discriminator (mV)	CPM	Clock Time	CPM	Clock Time
2.5	28307	9:43	52340	9:52
5	26178	9:45	46918	9:53.5
10	24989	9:46.5	46700	9:55
25	21848	9:48	40575	9:56.5
50	17462	9:49.5	32959	9:58
		Manganese		
Discriminator (mV)	Counts/ 2 min	Clock Time	Counts/ 2 min	Clock Time
2.5	9024	10:01	10312	10:14.5
5	8368	10:03.5	9758	10:17
10	7383	10:06	9232	10:19.5
25	6465	10:08.5	7862	10:21
50	4737	10:11	5962	10:23.5
		Tungsten		
Discriminator (mV)	Counts/ 5 min	Clock Time	Counts/ 5 min	Clock Time
2.5	500	10:20	886	10:45
5	489	10:25	861	10:50
10	447	10:30	840	10:55
25	414	10:35	727	11:00
50	326	10:40	624	11:05
		Gold		
Discriminator (mV)	Counts/ 5 min	Clock Time	Counts/ 5 min	Clock Time
2.5	2513	11:15	3922	11:40
5	2450	11:20	3486	11:45
10	2298	11:25	3511	11:50
25	2147	11:30	3042	11:55
50	1739	11:35	2612	12:00

Table 6. Sample processing of data for the indium foil

Discriminator (mV)	Count rate (cpm)	Net count rate (cpm)	Time since end of irradiation (min)	$e^{\lambda t}$	CPM * (cpm)	Count rate at 0 discr. setting (cpm)
			Outer foil			
2.5	28307	28292	8	1.108	31350	
5	26178	26163	10	1.137	29700	
10	24989	24974	11.5	1.159	29000	31300
25	21848	21833	13	1.182	25800	
50	17462	17447	14.5	1.204	21000	
			Inner foil			
2.5	52340	52325	17	1.243	65000	
5	46918	45903	18.5	1.268	58200	
10	46700	46685	20	1.292	60400	66800
25	40575	40560	21.5	1.318	53500	
50	32959	32944	23	1.343	44300	

activities were then corrected for decay since there was a time lag between the end of irradiation and the start of counting. The result after these two corrections is indicated by CPM*. This latter quantity was then plotted versus discriminator setting for both inner and outer foils. This is shown in Figure 6. The best lines were drawn through the two sets of data points and extrapolated back to zero. The extrapolated activities shown in the last column of Table 6 were then used to determine the flux.

A sample calculation of the flux at the resonance energies is shown in Table 7. The differences between the extrapolated activities of the outer and inner foils were corrected to saturation activity. In this correction the half-life of the neutron generator target is taken into account as well as the half-lives of the foil materials and the irradiation time of thirty minutes. The saturated activity differences were then corrected for self-absorption by using the factor f_s from Table 4. An area correction was made on the manganese activity to normalize it to the same area with the other foils. Finally, the flux correction factor was used. This factor was obtained by solving Equation 22 for the flux. The summation sign was dropped since the foils that were used have only one dominant resonance. The calculation of this correction factor is shown in Table 8.

The relative fluxes for this set of data are indicated

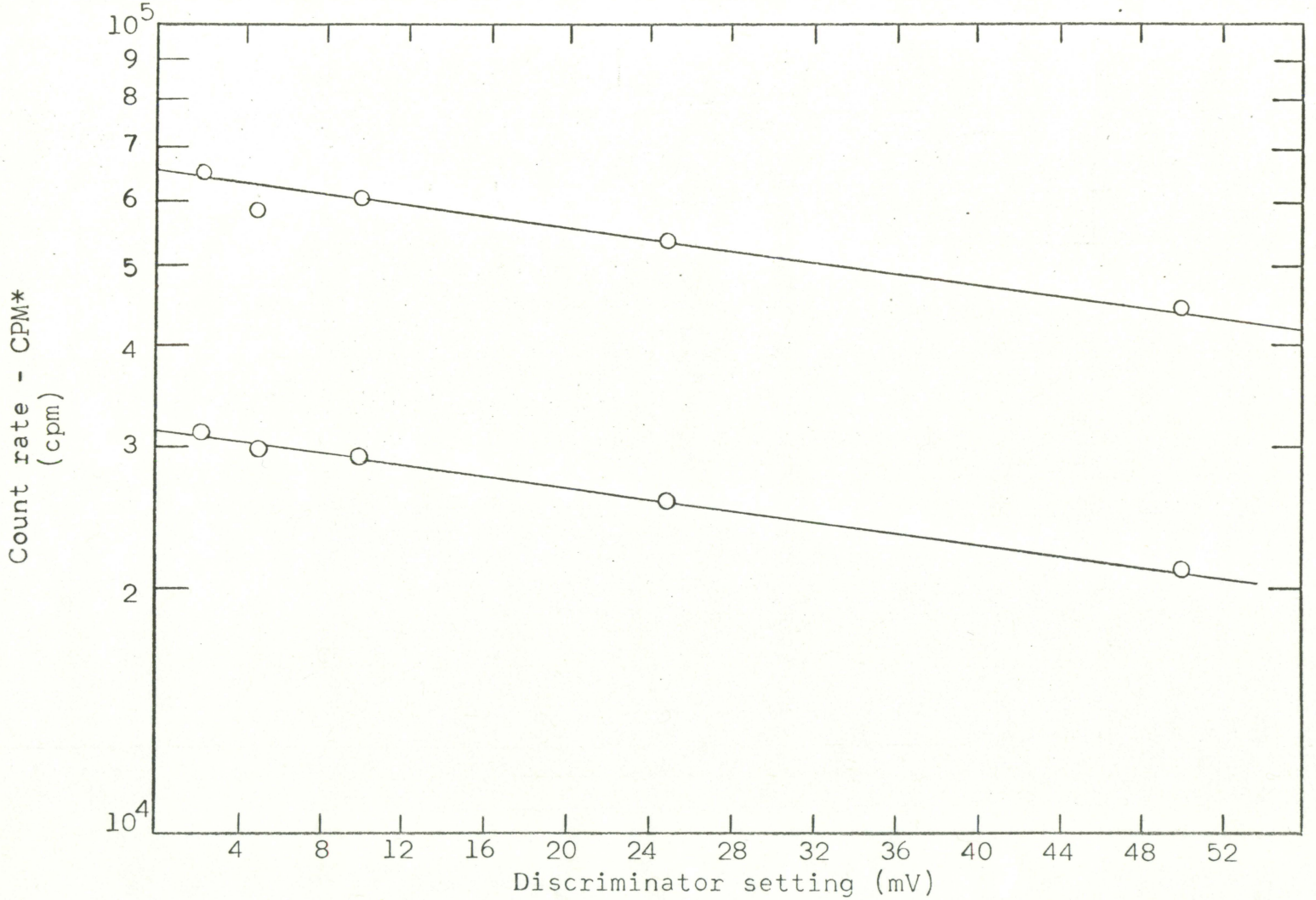

Figure 6. Counting rate versus discriminator setting for indium

Table 7. Sample calculation of relative flux[a]

Material	Zero discriminator count rate: Outer Foil (cpm)	Zero discriminator count rate: Inner Foil (cpm)	Difference in count rate (cpm)	Saturation correction factor	f_s	Area factor	Flux correction factor	Relative flux ($\frac{n}{cm^2 sec\ eV}$)
In	31300	66800	35500	3.27	0.698	1.0	8.89	1,475,000
An	500	740	240	195	0.670	1.0	6.58	460,000
W	87	172	85	72.5	0.562	1.0	25.4	278,000
Mn	4700	6200	1500	8.26	0.254	0.89	.715	31,000

[a]Relative flux =

$$\frac{\text{(Difference in count rate)(Saturation factor)(Area factor)(Flux factor)}}{\text{(Self absorption factor)}}.$$

Table 8. Calculation of the flux correction factor[a]

Material	Thickness (in.)	Γ_γ (eV)	Height of resonance (barns)	$M=t\Sigma_{t\ max}$	2I(M)	I(2M)	Flux correction factor
In^{115}	0.002	0.072	30,000	5.55	22	15.8	8.89
Au^{197}	0.001	0.124	30,000	4.47	19	14.1	6.58
W^{186}	0.001	0.045	14,000	2.22	13.0	9.5	25.4
Mn^{55}	0.024	0.5	3,400	16.3	38.2	27	.715

[a]Flux correction factor = $[\frac{1}{4}\Gamma_\gamma(2I(M) - I(2M))]^{-1}$.

in the last column of Table 7. It should be stressed that these values are not correct in an absolute sense because absolute counting rate measurements were not performed. The stated fluxes represent relative measurements.

The final results of the experiment are shown in Table 9. Here the measured fluxes are shown for the three paraffin slabs used. The first two runs pertain to the same slab. This measurement was repeated in order to check the consistency of the measurements and to obtain a measure of the variations and errors induced. The other runs were normalized to the first run in order to make comparison of the flux shapes more meaningful.

One of the basic aims of the experiment was to see whether, in the energy region 1 to 350 eV, the flux could be expressed by an exponential function of the form $\emptyset = AE^{-\sigma}$ where A and σ are positive constants. The data shown in Table 9 were plotted on logarithmic paper to determine if they could fit a straight line. This plot is shown in Figure 7. The data seemed to fit an exponential type relationship fairly well and therefore a logarithmic least-squares fit was made to the data obtained in each run. The equations resulting from this least-squares fit are shown at the right of Table 9.

The absolute values for σ of the exponents for the two runs using the slab thickness agree to within two percent.

Table 9. Relative flux measurements at the resonance energy of four resonance absorbers

Run	Slab thickness (in.)	Flux at In res. $(\frac{n}{cm^2 sec\ eV})$	Flux at Au res. $(\frac{n}{cm^2 sec\ eV})$	Flux at W res. $(\frac{n}{cm^2 sec\ eV})$	Flux at Mn res. $(\frac{n}{cm^2 sec\ eV})$	Energy dependence of spectrum
1	2.5 = $0.69\lambda_s$	1,685,000	740,000	377,000	38,800	$\phi = 2.33 \times 10^6 E^{-0.689 \pm 0.014}$
2	2.5 = $0.69\lambda_s$	1,685,000	791,200	376,300	42,800	$\phi = 2.34 \times 10^6 E^{-0.674 \pm 0.013}$
3	1.87 = $0.518\lambda_s$	1,685,000	649,000	339,000	44,980	$\phi = 2.08 \times 10^6 E^{-0.654 \pm 0.013}$
4	1.25 = $0.345\lambda_s$	1,685,000	525,000	317,500	35,400	$\phi = 2.2 \times 10^6 E^{-0.724 \pm 0.014}$

Figure 7. Relative flux versus neutron energy

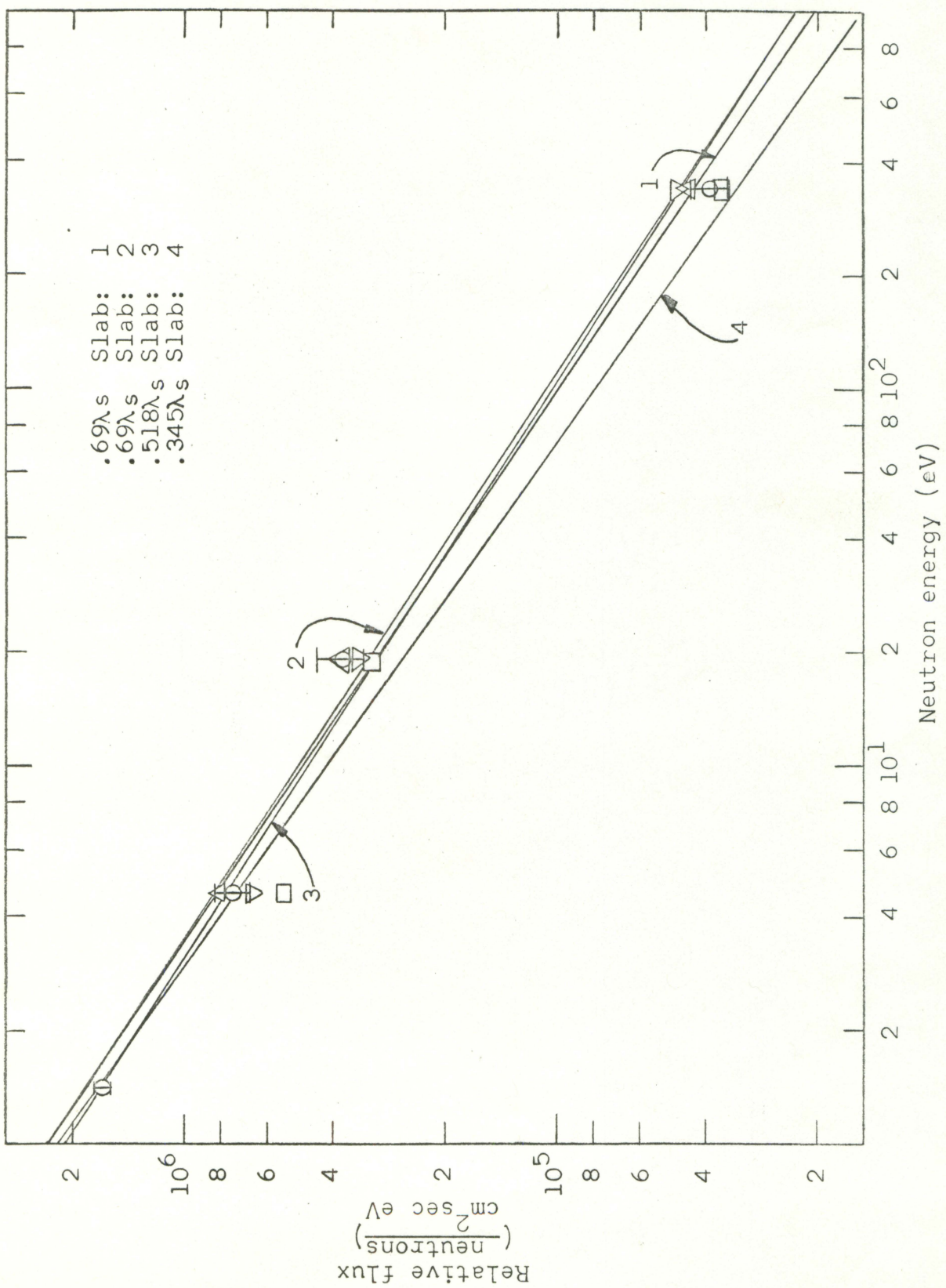
.69λs Slab: 1
.69λs Slab: 2
.518λs Slab: 3
.345λs Slab: 4
Relative flux
(neutrons / cm² sec eV)
Neutron energy (eV)
2
4
6
8
10⁵
10⁶
10¹
10²

This is the same deviation obtained if counting statistics are taken into account, and if the range of the value for the slope for all straight lines that fit the points within one standard deviation is obtained.

The average value of σ for the first two runs was 0.682. This value was compared with results obtained by Michaudon (9) who used a Monte-Carlo technique to obtain the neutron spectrum exiting from a moderating slab. The slab thickness used in his work was four scattering mean free paths. His results give an exponential relationship with a value for σ of 0.83. It must be noted that this value cannot be directly compared with the results obtained in the experiments reported in this thesis because of the difference in moderator thickness. It was impossible to carry out measurements at the thickness used in Michaudon's calculations because of the large amount of paraffin required.

It is, however, possible to compare the two results in a qualitative manner. It should be expected that as the slab thickness is increased σ would approach a value of 1.0. Since the slab used for the experiments described in this thesis was thinner than the slab used by Michaudon, it should be expected that his σ value would be closer to the limiting value of 1.0 than the value obtained in this thesis, as is indeed the case. Thus the difference in the two results seems to be in the right direction.

All three σ values plotted versus slab thickness are shown in Figure 8. For the first two runs the average value of σ is plotted. The results obtained when the thinner slabs were used seems to be contradictory. The σ value for the $0.518\lambda_s$ thick slab is less than the σ value for the $0.69\lambda_s$ thick slab as one might expect, but for the even thinner slab, $0.345\lambda_s$, σ is larger than in either of the previous cases. The trend should be towards smaller values for σ as the slab becomes thinner and the number of neutrons which are moderated into the epithermal energy region is decreased in favor of higher energy neutrons. The failure of σ for the $0.345\lambda_s$ thick slab to decrease with respect to the thicker slabs leads the author to believe that this σ value is in error. This error could have been the result of difficulty in maintaining the proper geometry for the thinner slabs. It could also have been caused by the failure of the assumption that the neutrons are isotropic. This assumption becomes more and more questionable as the slab gets thinner. Furthermore, it is questionable whether the differences observed between the three σ values, σ_1, σ_2, σ_3 for the three slabs in order of decreasing thickness, are statistically significant. For example, σ_2 is only smaller than σ_1 by two standard deviations which is just on the border line to make it different than σ_1 in a statistically significant way. On the other hand, σ_3 is three standard deviations higher

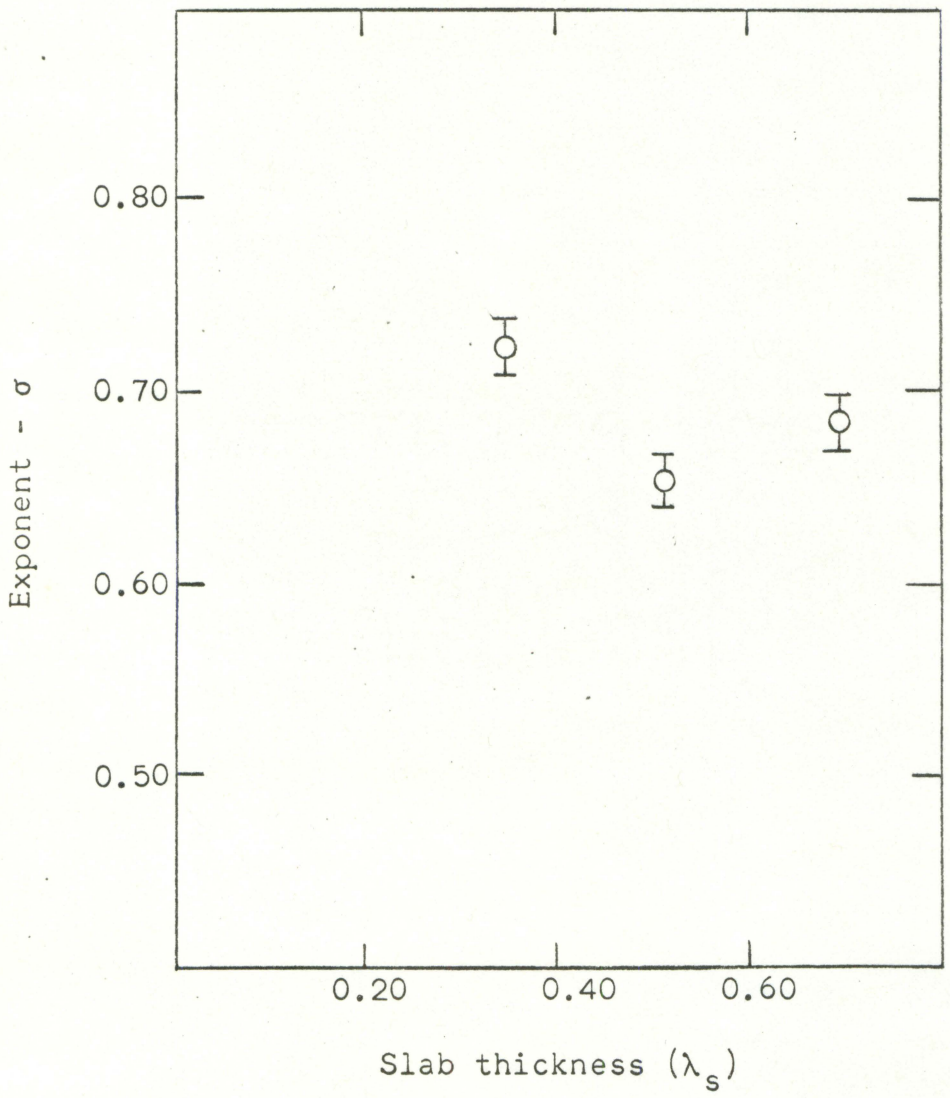

Figure 8. Exponent versus slab thickness

than σ_i but its magnitude goes in the wrong direction from a physically plausible point of view.

Due to time limitations it was impossible to carry out measurements with a wider range of slab thicknesses. Such an extension of the measurements would be very useful in determining, to a greater degree, the dependence of σ on slab thickness. It can be concluded, however, that the exponent does not change rapidly as the slab thickness is changed. This can be seen from the results of Michaudon. The value for σ of 0.83 computed by Michaudon for a slab thickness of four mean free paths is only 0.148 higher than the average σ obtained in this thesis for a slab thickness of 0.69 mean free paths. Therefore for small thickness variations as those used in these experiments one would not expect to see a considerable variation in σ. Experiments with a wider range of thickness, from 0.5 to 5 mean free paths, would be necessary to detect unambiguously the trends in σ with thickness variation.

VI. SUMMARY AND CONCLUSIONS

The spectrum of neutrons exiting from a moderator slab was measured using source neutrons of high energy produced by a neutron generator. The spectrum was measured in the energy region 1 to 350 eV by the sandwich foil technique. This technique involved the use of four resonance materials placed in sandwiches. Each sandwich was used to determine the neutron flux at the resonance of that sandwich material. From the measured flux at the four different resonances a spectrum was obtained. Measurements were carried out for three different slab thicknesses to determine the effect of slab thickness on the exiting spectrum.

It was concluded that the sandwich foil technique is applicable to this type of measurement and gives meaningful results. The assumption that the neutron flux is isotropic seems to be correct in all but the thinnest slab. It was also concluded that the neutron flux varies exponentially with neutron energy in the energy range that was studied and that the absolute value of the exponent decreases slowly with decreasing thickness, although this trend was not established unambiguously due to the limited range of thickness used.

VII. TOPICS FOR FURTHER STUDY

While the question of the spectrum in the 1 to 350 eV range has been basically answered, many other related problems remain unsolved. Some of these problems deserve attention.

The spectrum above 350 eV is an excellent topic for study. The higher energies above 80 KeV could be studied with the use of a Bennet spectrometer or possibly threshold reactions. The energy region between 1 and 80 KeV also merit study and perhaps new techniques could be developed to measure the spectrum in this energy region.

The effect of the geometrical configuration on the spectrum could be studied in more detail. Slabs of different thicknesses, shape and material could be used in conjunction with the sandwich technique to determine the effect of these parameters on the spectrum in the 1 to 350 eV range. Measurements could be carried out to determine what effect, if any, angular dependence has upon the spectrum and compared to similar results obtained by Michaudon (9).

The sandwich foil technique could be adapted to the reactor to measure its neutron spectrum in the indicated energy range. This method offers possible advantages over the normally employed cadmium ratio technique.

Finally the sandwich foil technique offers a possible

method of making time dependent spectrum measurements through the use of prompt gamma emission. This method would be especially attractive to investigate the features of a moderated pulse produced through a moderator slab from a fast neutron pulse generator. Such an arrangement might be an inexpensive way to produce and study thermal or epithermal neutron pulses without the need of a reactor and complicated chopper equipment. The measurements could be done by measuring the prompt γ rays produced by just one foil and then by a sandwich. The difference between the number of prompt γ rays measured for the sandwich, and the γ rays for a single foil would correspond to the prompt γ ray emission of the outer foil. Thus it would be possible to obtain reaction rates for both an inner and outer foil just as in the experiment that was performed in this thesis. The difference would be that now time dependent effects could possibly be measured since the γ rays would be prompt. It is possible that background radiation and low intensity might make it difficult to obtain meaningful results, but the method is worth trying.

VIII. LITERATURE CITED

1. Bennett, E. F. Proportional counter proton-recoil spectrometer with gamma discrimination. Review of Scientific Instruments 33: 1153-1160. 1962.

2. Bothe, W. Zur Methodik der Neutronen Sonden. Zeitschrift Für Physik 120: 437-449. 1943.

3. Ehret, G. Die Bestimmung epithermischer Neutronenspektren mit Resonanzonden (sandwich methode). Atompraxis 7: 393-400. 1961.

4. Goldberg, M. D., Mughabghab, S. F., Magurno, B. A., and May, V. M. Neutron cross sections. United States Atomic Energy Commission Report BNL 325, Second edition, Supplement No. 2, Volume IIA, Z = 21 to 40 (Physics - TID-4500) [Brookhaven National Laboratory, Upton, New York] 1966.

5. Goldberg, M. D., Mughabghab, S. F., Purohit, S. N., Magurno, B. A., and May, V. M. Neutron cross sections. United States Atomic Energy Commission Report BNL 325, Second edition, Supplement No. 2, Volume IIB, Z = 41 to 60 (Physics - TID-4500) [Brookhaven National Laboratory, Upton, New York] 1966.

6. Goldberg, M. D., Mughabghab, S. F., Purohit, S. N., Magurno, B. A., and May, V. M. Neutron cross sections. United States Atomic Energy Commission Report BNL 325, Second edition, Supplement No. 2, Volume IIC, Z = 60 to 87 (Physics - TID-4500) [Brookhaven National Laboratory, Upton, New York] 1966.

7. Huber, R. J. In core experiments with a lithium-6 sandwich fast neutron spectrometer. American Nuclear Society Transactions 7: 368-369. 1964.

8. Judd, A. M. Neutron flux measurements by resonance activation of foils. Nuclear Instruments and Methods 23, No. 1: 29-35. 1963.

9. Michaudon, A. The production of moderated neutron beams from pulsed accelerators. Reactor Science and Technology (Journal of Nuclear Energy Parts A/B) 17: 165-186. 1963.

10. Price, W. J. Nuclear radiation detection. 2nd ed. McGraw-Hill Book Co., Inc., New York, N.Y. 1964.

11. Prud'homme, J. T. Texas Nuclear Corporation neutron generators. Texas Nuclear Corp., Austin, Texas. 1962.

12. Reactor laboratory experiments: Neutron flux measurements by induced activation methods. International Institute of Nuclear Science and Engineering, Argonne National Laboratory, Argonne, Ill. 1963.

13. Young, J. C., Trimble, G. D., Naliboff, Y. D., Houston, D. H., and Beyster, J. R. Neutron spectrum measurements in H_2O, CH_2, and C_6H_6. Nuclear Science and Engineering 18: 376-399.

IX. ACKNOWLEDGMENTS

The author wishes to thank the various members of the Nuclear Engineering staff. In particular the author would like to thank Dr. Achilles G. Adamantiades for his original suggestion of this project and his continued active interest and help. To Dr. Glenn Murphy are due the authors deepest thanks for his guidance and encouragement.

The author wishes to thank the National Aeronautics and Space Administration for the fellowship under which this work was done.

Finally, the author wishes to thank his parents for their unending patience and encouragement they have given him.